Science
AAAS

Creating Long-Lived Superhydrophobic Polymer Surfaces Through Mechanically Assembled Monolayers

Jan Genzer, *et al.*

Science **290**, 2130 (2000);
DOI: 10.1126/science.290.5499.2130

Science (print ISSN 0036-8075; online ISSN 1095-9203) is published weekly, except the last week in December, by the American Association for the Advancement of Science, 1200 New York Avenue NW, Washington, DC 20005.

Creating Long-Lived Superhydrophobic Polymer Surfaces Through Mechanically Assembled Monolayers

Jan Genzer* and Kirill Efimenko

We show that elastomeric surfaces can be tailored using "mechanically assembled monolayers" (MAMs), structures that are fabricated by combining self-assembly of surface grafting molecules with mechanical manipulation of the grafting points in the underlying elastic surface. The versatility of this surface modification method is demonstrated by fabricating MAMs with semifluorinated (SF) molecules. These SF-MAMs have superior nonwetting and barrier properties in that they are "superhydrophobic" and nonpermeable. We also establish that these material characteristics do not deteriorate even after prolonged exposure to water, which usually causes surface reconstruction in conventionally prepared SF self-assembled monolayers.

The surface properties of materials, such as wetting and lubrication, can be successfully tailored by terminally attaching various organic modifiers. In particular, deposition of self-assembled monolayers (SAMs) offers one of the highest quality routes used to prepare chemically and structurally well-defined surfaces (*1*, *2*). Appropriate and useful application of SAMs requires understanding of molecular level organization of the SAM chains. The wetting properties of SAMs and their stability are governed by the intimate interplay between the chemical nature of the terminus of the monolayer molecule (ω-) and the packing within the SAM (*3*). The latter in turn influences the in-plane arrangement of the ω-functionalized surface groups.

The packing density of the SAMs not only determines their surface energies but ultimately influences the stability of the monolayer and its resistance to surface reconstruction (*1*, *4*). For example, monolayers of SF SAMs can be routinely prepared that have surface energies of ≈8 mJ/m^2, a value near that of a perfectly close-packed crystalline array of $-CF_3$ groups (≈6 mJ/m^2) (*3*, *4*–*8*). However, when exposed to polar liquids, such as water, these SF-SAMs usually lose their low-energy surface properties because the water molecules penetrate through the imperfections in the SF-SAMs, causing this surface to reconstruct (*4*).

These nondesirable surface reconstruction effects can likely be minimized (or even completely prevented from occurring) by increasing the packing density of the SAMs through increasing the density of the grafting points at the surface. However, tailoring the grafting density of the SAM chains is not an easy task. SAMs are usually formed through self-assembly processes that are governed by the chemical and structural nature of the SAM molecules and the means of their attachment to the substrate. In this report, we show that the grafting density and thus the chain packing can be successfully tailored when combined with mechanical manipulation of the attachment points of the molecules at the substrate. Specifically, we demonstrate that the combination of the self-assembly with mechanical manipulation of the grafted molecules on surfaces provides a means of fabricating MAMs ("mechanically assembled monolayers") that form superhydrophobic surfaces with superior long-lasting barrier properties.

The method for fabricating MAMs is based on combining (i) the grafting reaction between SF trichlorosilanes, $F(CF_2)_y(CH_2)_xSiCl_3$(FyHx), and hydroxyl functionalities present at silica surfaces,

$$F(CF_2)_y(CH_2)_xSiCl_3 + 3H_2O \xrightarrow{-3HCl} F(CF_2)_y(CH_2)_xSi(OH)_3 \quad (1)$$

$$F(CF_2)_y(CH_2)_xSi(OH)_3 + HO-[Si]_{substrate} \xrightarrow{-3H_2O} F(CF_2)_y(CH_2)_xSi \equiv O-[Si]_{substrate} \quad (2)$$

and (ii) mechanical manipulation of the HO-$[Si]_{substrate}$ groups. To accomplish the latter, the surface –OH functionalities are created by ultraviolet/ozone (UVO) treatment of a poly(dimethyl siloxane) (PDMS) network film that has previously been mechanically stretched, as shown schematically in Fig. 1. The major advantage of this technique over others is that much higher surface grafting densities of the assembling molecules can be achieved. Because PDMS behaves as an ideal elastic material in terms of its stress-strain response, the density of the HO-$[Si]_{surface}$ groups created by the UVO treatment and thus the degree of packing within the MAM are directly proportional to Δx and can be varied with precision over a very broad range (*9*).

We fabricated F6H2-MAM and F8H2-MAM by depositing $F(CF_2)_6(CH_2)_2SiCl_3$ and $F(CF_2)_8(CH_2)_2SiCl_3$, respectively, on PDMS-UVO substrates prepared by exposing PDMS network films (stretched previously by Δx) to UVO for 1 hour. As the PDMS substrate extension, Δx, increases, the advancing water contact angle, θ_w, increases (hydrophobicity of the surfaces increases) for both molecules, reaches a maximum at $\Delta x \approx$ 95%, and then decreases slightly for $\Delta x >$ 95% (Fig. 2A). The corresponding water contact hysteresis (the difference between the advancing and receding water contact angles) decreases with increasing Δx, reaches a minimum at around $\Delta x \approx$ 60%, and then increases for $\Delta x >$ 70% (Fig. 2B). The results presented in Fig. 2 indicate the packing of the FyH2 molecules in the FyH2-MAMs. As Δx increases from 0%, the number of the FyH2 groups per unit area increases, which in turn results in closer chain packing within the MAM. At $\Delta x \approx$ 60 to 70%, the molecules are already densely packed. With $\Delta x >$ 70%, the molecules in the MAM must begin to corrugate as a layer. This response gives rise to an enhanced molecular roughness and causes the contact angle hysteresis to increase. The data in Fig. 2 also show that θ_w for F8H2 is higher than that for F6H2; thus, the hydrophobicity of the FyH2-MAMs improves with increasing *y*. This effect is presumably associated with better chain alignment and packing of the longer FyH2 moieties.

We can use the data in Fig. 2 to estimate the grafting density of the FyHx groups on the PDMS-UVO surfaces. Realizing that the $-(CF_2)-$ part of the molecule forms a three-dimensional helix with a diameter of ≈0.56 nm (*10*) and assuming that these chains are close packed at $\Delta x \approx$ 65%, a grafting density of ≈1.5 × 10^{14} molecules/nm^2 can be estimated from a simple geometry. This value is reasonable considering that the density of –OH groups on carefully prepared silicon dioxide on top of a silicon wafer is ≈5 × 10^{14} molecules/nm^2 (*11*).

We used near-edge x-ray absorption fine structure (NEXAFS) to study the molecular orientation of the MAMs surfaces (*12*, *13*). NEXAFS involves the resonant x-ray excitation of a K or L shell electron to an unoccupied low-lying antibonding molecular orbital of σ symmetry, σ* (and π symmetry, π*) (*14*). The initial state K shell excitation gives element specificity, whereas the final state unoccupied molecular orbitals provide bonding or chemical selectivity. Because of the fixed geometry and governing of the 1s → σ* (and 1s

Department of Chemical Engineering, North Carolina State University, Raleigh, NC 27695–7905, USA.

*To whom correspondence should be addressed. E-mail: jan_genzer@ncsu.edu

$\rightarrow \pi^*$) excitations by dipole selection rules, the resonance intensities vary as a function of the direction of the electric vector **E** of the incident polarized x-ray relative to the symmetry of the molecule (*15*). The NEXAFS experiments were carried out on the NIST/Dow soft x-ray materials characterization facility at the National Synchrotron Light Source at Brookhaven National Laboratory (NSLS BNL) (*16*). The setup at NSLS BNL is capable of measuring both the partial electron yield (PEY) NEXAFS and the fluorescence yield (FY) NEXAFS spectra. By simultaneously detecting both the PEY and FY NEXAFS signals, whose probing depths are ≈2 and ≈100 nm, respectively, the orientation of the molecules on the surface and in the interior of the sample can be resolved.

No measurable fluorine signal could be detected in the FY NEXAFS spectra of the SF-MAMs, suggesting that the UVO treatment and subsequent MAMs deposition did not modify the interior of the PDMS. However, the PEY NEXAFS data revealed a strong peak at 292.0 eV, corresponding to the $1s \rightarrow \sigma^*_{CF}$ (*12*, *13*, *17*). The orientation of the SF molecules in the SF-MAMs was inferred by monitoring the dependence of the intensity of the $1s \rightarrow \sigma^*_{CF}$ transition on the sample orientation. Specifically, the PEY NEXAFS spectra were collected at eight different angles θ ranging from 20° to 90°, where θ is the angle between the sample normal and the polarization vector of the x-ray beam. A more quantitative analysis with models presented elsewhere (*12*, *13*) reveals that the average tilt angles of the fluorocarbon helix (*18*), $<\tau_{F\text{-}helix}>$, measured along and perpendicular to the stretching direction on the F8H2-MAM sample prepared on unstretched PDMS-UVO substrate, are ≈5° and ≈4°, respectively, which is in accord with the orientation of F8H2-SAM deposited on a SiO_x substrate (*12*, *13*). The analysis of the PEY NEXAFS spectra from F8H2-MAM with Δx = 70% reveals that $<\tau_{F\text{-}helix}>$ measured along the stretching direction is ≈38° and $<\tau_{F\text{-}helix}>$ collected perpendicular to the stretching direction is ≈21°. The NEXAFS experiments thus show that as Δx increases, the F8H2 chains tilt away from the sample normal in the stretching direction. Increase of $<\tau_{F\text{-}helix}>$ from ≈4° to ≈21° as Δx increases from 0 to 70% can be attributed to the slight compression of the sample perpendicular to the uniaxial stretch.

As mentioned above, fluoroalkyl-containing monolayers represent an industrially important class of materials. These structures can be used to fabricate surfaces with the lowest possible surface energies (*3*, *4*–*8*), which facilitate biocompatibility. Depositing semifluorinated moieties on flexible substrates, like PDMS, may be beneficial in cases where one needs to have deformable substrates, such as the case of implants that require a certain degree of mechanical flexibility (*19*, *20*). In addition, it has been found that PDMS-based supports are advantageous for marine coatings—the flexibility of these materials contributes greatly to their ability of being easily cleaned of fouling (*21*, *22*). However, when exposed to polar liquids, these materials usually reconstruct at their surface and lose their low-energy surface properties. This surface reconstruction can be minimized or completely avoided in the MAMs because the FyHx chains can be mechanically manipulated to form very closely packed arrays. We designed a series of experiments aimed at exploring the resistance of the FyHx-MAMs to surface reconstruction.

The samples were prepared as previously described, immersed in water for controlled time intervals, and then dried with nitrogen. Figure 3 shows the advancing water contact angles, θ_w, of F6H2-MAMs (squares) and F8H2-MAMs (circles) prepared on PDMS-UVO substrates with Δx = 0% (solid symbols) and Δx = 70% (open symbols) after exposure to water. Regardless of *y*, the θ_w on the FyH2-MAM fabricated on the unstretched substrate drops almost immediately after a short water exposure, which indicates that the FyH2 chains surface reconstruct. However, θ_w on the FyH2-MAM samples prepared on PDMS-UVO with Δx = 70% decreases only slightly with water exposure time. For example, after water immersion for 7 days, θ_w on F6H2-MAM and F8H2-MAM decreases only by ≈5°, which represents the respective decreases in water contact angle of 4.0 and 3.8% from the values measured before the water exposure. To check on the ability of the FyHx-MAMs to resist surface reconstruction, we placed the FyH2-MAM (Δx = 70%) samples in a plastic Petri dish and left them under ambient laboratory conditions (with no control of humidity or temperature) for 6 months. The crossed symbols in Fig. 3 show the θ_w values measured on these samples. A close inspection of the data in Fig. 3 reveals that during the 6-month "incubation" period, the wettability of the

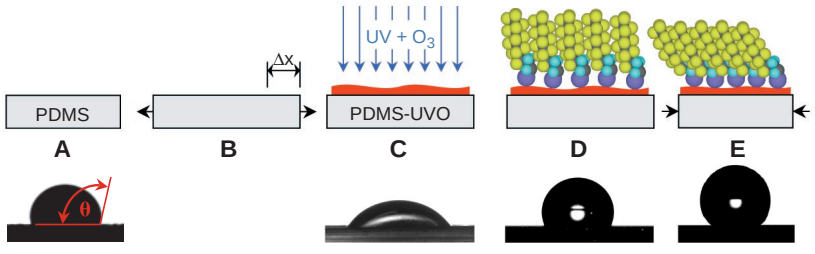

Fig. 1. Top panels are schematics illustrating the technological steps leading to the production of MAMs. (**A**) A pristine PDMS network film is prepared by casting a mixture of PDMS and a cross linker (*24*, *29*, *30*) into a thin (≈0.5 mm) film and curing it at 55°C for about 1 hour. (**B**) After soxhlet extraction in chloroform for 24 hours, which removes any non–cross-linked PDMS oligomers, the film is cut into small strips (≈1 × 5 cm^2) and mechanically stretched by a certain length, Δx. Subsequent exposure to a UVO treatment (*24*–*26*, *30*) produces hydrophilic PDMS surfaces (PDMS-UVO) composed mainly of hydroxyl groups as revealed from Fourier transform infrared and NEXAFS experiments (*27*). (**C**) By increasing the length of the UVO treatment, the number of the surface hydrophilic groups increases, causing the water contact angle to decrease. The HO-$[Si]_{surface}$ groups are particularly important because they serve as attachment points for the chlorosilane molecules. (**D**) The FyHx molecules are deposited from vapor (*31*) onto this stretched substrate and form an organized SAM. (**E**) Finally, the strain is released from the PDMS-UVO film, which returns to its original size, causing the grafted FyHx molecules to form a densely organized MAM. To remove weakly physisorbed FyHx molecules, we wash the samples thoroughly in warm (≈60°C) distilled water for 1 min and dry them with nitrogen. The bottom panels show photographs of a water droplet spreading on each of the substrates.

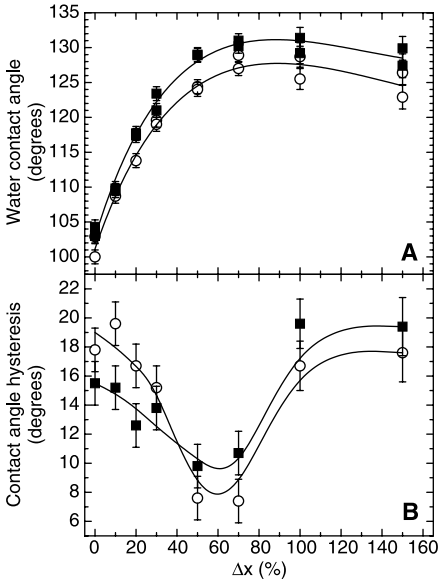

Fig. 2. (**A**) The dependence of the water contact angle, θ_w, on F6H2-MAM (circles) and F8H2-MAM (squares) samples on the degree of stretching of the PDMS substrate before the UVO treatment, Δx. (**B**) The corresponding contact angle hysteresis (defined as the difference between the advancing and receding water contact angles). The lines are meant to guide the eye (*32*). Symbols as in (A).

F6H2-MAM and F8H2-MAM samples decreased only by ≈7° and ≈3.5°, respectively, for "as-prepared" samples and ≈10° and ≈5°, respectively, for samples immersed in water for 7 days. Moreover, by comparing the data from the MAMs deposited on the stretched substrates, it is evident that the MAMs made of the longer fluorocarbon chain exhibit better stability and resistance to polar environment. This response is presumably associated with better packing of the longer SF moieties as compared with the shorter SF groups.

Our results are in accord with previous work by Wang and co-workers on surfaces made of poly(styrene-isoprene) block copolymers with attached FyHx pendent groups that formed SF-SAMs (*4*). Wang and coworkers also observed that the surface hydrophobicity and stability increased as the fluorocarbon length increased from F6H10 to F10H10. Comparing our results on F6H2-MAM and F8H2-MAM samples with those of Wang using F6H10 and F8H10 groups reveals that the FyH2-MAMs remain more hydrophobic (by ≈6° and ≈49°, respectively) after prolonged exposures to water. We attribute this behavior to the means of ordering of the FyHx molecules, which ultimately defines the chain packing and mobility. Although the organization of the FyHx groups on the surfaces of SF polymer films is controlled by materials self-assembly (*3*), the mechanical manipulation of the molecules in the SF-MAMs causes the FyHx moieties to be more closely stacked and interlocked (*23*). To validate the close packing and the resulting low mobility of the FyH2 molecules on the surfaces of the SF-MAMs, we carried out NEXAFS experiments on F8H2-MAM samples with $\Delta x = 0\%$ and $\Delta x = 70\%$ that were exposed to water for the same time intervals.

Figure 4 shows the values of the average tilt angles of the fluorocarbon helix, $<\tau_{\text{F-helix}}>$, that were determined from PEY NEXAFS spectra collected from F8H2-MAMs with $\Delta x = 0\%$ (squares) and $\Delta x = 70\%$ (circles). As mentioned earlier in this report, the F8H2-MAMs prepared on unstretched PDMS-UVO substrates ($\Delta x = 0\%$) stand almost perpendicular to the sample surface. However, the data in Fig. 4 show that when exposed to water, the chain orientation starts to disappear very rapidly, and after about 1 day of water exposure, the F8H2-MAMs with $\Delta x = 0\%$ disorient completely. The response of the F8H2-MAMs prepared on PDMS-UVO substrates with $\Delta x = 70\%$ is very different. Specifically, the NEXAFS data reveal that $<\tau_{\text{F-helix}}>$ on samples exposed to water for up to 7 days is indistinguishable from that measured on the same specimen before the water exposure. These results thus provide further evidence that the F8H2 molecules in MAMs with $\Delta x = 70\%$ are closely packed and mechanically interlocked; this interlocking hinders the chain's tendency to move and reconstruct on the MAM surface.

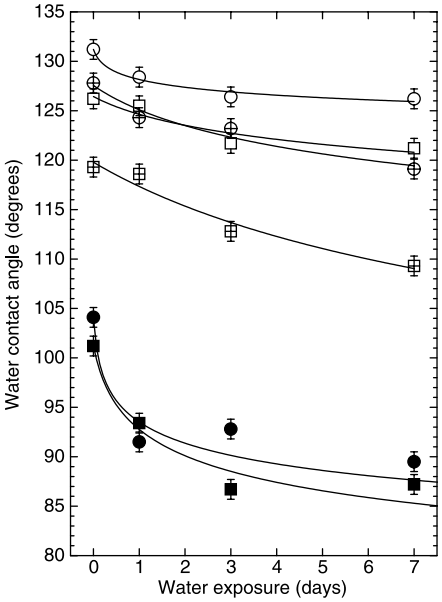

Fig. 3. The dependence of the water contact angle, θ_w, of F6H2-MAM (squares) and F8H2-MAM (circles) on the exposure time of the FyHx-MAMs to water. The solid symbols denote the contact angles measured on FyH2-MAMs with $\Delta x = 0\%$. The open symbols mark the contact angles measured on FyH2-MAMs with $\Delta x = 70\%$ taken immediately after the water exposure and substrate drying with nitrogen. The crossed symbols represent the contact angles from the samples denoted by the open symbols but measured 6 months later (the samples were stored under ambient laboratory conditions in Petri dishes with no temperature or humidity control between the water exposure and the measurement). The lines are meant to guide the eye.

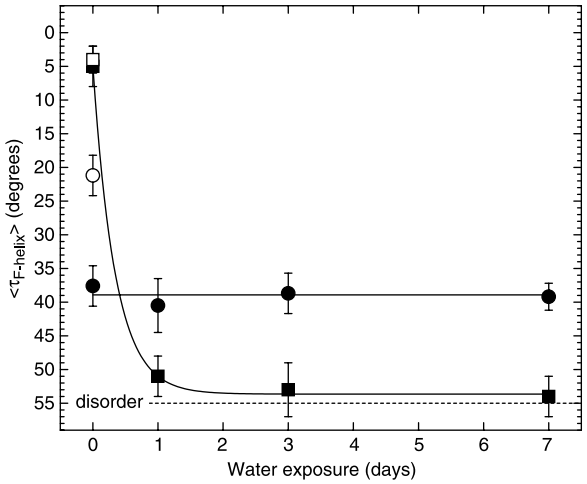

Fig. 4. The dependence of the average tilt angle of the fluorinated helix, $<\tau_{\text{F-helix}}>$, in F8H2-MAMs on the exposure time of the F8H2-MAM to water. The squares and circles denote $<\tau_{\text{F-helix}}>$ in F8H2-MAM ($\Delta x = 0\%$) and F8H2-MAM ($\Delta x = 70\%$) samples, respectively. The solid and open symbols represent $<\tau_{\text{F-helix}}>$ measured along and perpendicular to, respectively, the stretching direction. The dashed line marks the value of $<\tau_{\text{F-helix}}>$ corresponding to a completely disoriented MAM. The solid lines are meant to guide the eye.

References and Notes

1. A. Ulman, *An Introduction to Ultrathin Organic Films from Langmuir-Blodgett to Self Assembly* (Academic Press, New York, 1991).
2. M. K. Chaudhury, *Mat. Sci. Eng. Rep.* **16**, 97 (1996).
3. Depending on the chemical nature of ω-, the surface properties of the SAMs range from hydrophobic to hydrophilic.
4. J. Wang, G. Mao, C. K. Ober, E. J. Kramer, *Macromolecules* **30**, 1906 (1997).
5. J. D. Swalen *et al.*, *Langmuir* **3**, 932 (1987).
6. M. K. Chaudhury, G. M. Whitesides, *Science* **255**, 1230 (1992).
7. M. K. Chaudhury, *Curr. Opin. Coll. Int. Sci.* **2**, 65 (1997).
8. ———, *Biosens. Bioelectron.* **10**, 785 (1995).
9. Experiments investigating the cooperative effects of sample stretching and the UVO treatment revealed that samples extended up to $\Delta x \approx 150\%$ and subsequently UVO treated always recovered their original length (with an error of 0.5% or smaller) after releasing the stress from the substrate.
10. E. D. Chidsey, D. N. Loiacono, *Langmuir* **6**, 682 (1990).
11. S. R. Wasserman, Y.-T. Tao, G. M. Whitesides, *Langmuir* **5**, 1074 (1989).
12. J. Genzer *et al.*, *Langmuir* **16**, 1993 (2000).
13. J. Genzer *et al.*, *Macromolecules* **33**, 1882 (2000).
14. J. Stöhr, *NEXAFS Spectroscopy* (Springer-Verlag, Berlin, 1992).
15. Because of the nature of the polarization dependencies of the NEXAFS signal intensities, one cannot distinguish between a completely disoriented sample and a sample whose chains are all tilted by 54.7°, the so-called "magic angle" (*14*).
16. D. A. Fischer *et al.*, *Appl. Surf. Sci.* **133**, 58 (1998).
17. See supplementary information (available at *Science* Online at www.sciencemag.org/cgi/content/full/290/5499/2130/DC1) for more details on NEXAFS and the PEY NEXAFS spectra from the SF-MAMs.
18. We note that the tilt angle determined from NEXAFS represents an average value. There is no straightforward way to discriminate between the case of all chains homogeneously tilted by the same angle and the case of a disordered system with a broad distribution of tilt angles. Hence, we express our results on the orientation of the SF moieties in terms of the average tilt angle of the fluorocarbon part of the single SF groups, $<\tau_{\text{F-helix}}>$.
19. J. J. Kennan *et al.*, *J. Biomed. Mater. Res.* **36**, 487 (1997).
20. J. H. Silver *et al.*, *Biomaterials* **20**, 1533 (1999).
21. E. Johnston *et al.*, *Macromolecules* **32**, 8173 (1999).
22. M. Anderson *et al.*, *Biofouling* **14**, 167 (1999).
23. Wang and co-workers attributed the rather large difference in θ_w (≈50°) on the F6H10 and F8H10 molecules exposed to water for 7 days to the lower stability of the smectic-A phase of F6H10 as compared with the smectic-B phase of the F8H10 (*4*). The much smaller difference in θ_w (≈7°) for F6H2-MAM and F8H2-MAM samples is a consequence of mechanical stacking rather than thermodynamic self-assembly of the FyH2 molecules.
24. H. Hillborg, U. W. Gedde, *IEEE Trans. Dielectrics Electr. Insul.* **6**, 703 (1999), and references therein.
25. W. T. S. Huck *et al.*, *Langmuir* **16**, 3497 (2000).
26. M. Ouyang *et al.*, *Chem. Mater.* **12**, 1591 (2000).

27. K. Efimenko, J. Genzer, in preparation.
28. N. Bowden, S. Brittain, A. G. Evans, J. W. Hutchinson, G. M. Whitesides, *Nature* **393**, 146 (1998).
29. The PDMS networks are prepared from the commercial PDMS Sylgard 184 and the curing agent 184 (Dow Corning). The PDMS:curing agent ratio is 10:1, as recommended by the recipe provided by the manufacturer.
30. Previously, oxygen plasma was used to produce thin layers of SiO_x on the PDMS surfaces (*24*). We chose UVO rather than an oxygen plasma because the UVO treatment, at the wavelength of $\lambda = 254$ nm, does not cover the surface of PDMS with a continuous SiO_x layer (*25*, *26*), as confirmed from combined experiments with a palette of experimental probes that included Fourier transform infrared spectrometry in the attenuated total reflection, NEXAFS, x-ray reflectivity, and contact angle measurements (*27*). Hence, the mechanical properties of the PDMS substrates are not altered as much as in the case of oxygen plasma–treated PDMS (*9*, *28*).
31. The SAM deposition experiments are usually done in a desiccator that is connected to a mechanical vacuum pump. The vacuum level in the deposition chamber is $\approx 10^{-2}$ to 10^{-3} torr, so that there is still a sufficient amount of water molecules needed for reaction 1. The sample is placed upside down above the diffusion source, which consists of a mixture of the chlorosilane and paraffin oil. Because the paraffin oil does not mix with the chlorosilane molecules, it provides a convenient dilutant medium for the diffusion source; the flux of the FyHx molecules can be conveniently adjusted by simply varying the FyHx: paraffin oil ratio.
32. Contact angle experiments were performed with a Ramé-Hart contact angle goniometer, model 100-00. The advancing contact angles were read by injecting 4 μl of deionized water; the receding contact angles were determined by removing 3 μl of deionized water from the droplet. Each data point reported here represents an average over four measurements on the same sample.
33. Supported by the North Carolina State University College of Engineering startup funds and the NSF CAREER award, grant DMR98-75256. NEXAFS experiments were carried out at the National Synchrotron Light Source, Brookhaven National Laboratory, which is supported by the U.S. Department of Energy, Division of Materials Sciences and Division of Chemical Sciences. We thank D. A. Fischer and W. E. Wallace for their assistance during the course of the NEXAFS experiments.

7 August 2000; accepted 8 November 2000

External Control of 20th Century Temperature by Natural and Anthropogenic Forcings

Peter A. Stott,[1]* S. F. B. Tett,[1] G. S. Jones,[1] M. R. Allen,[2] J. F. B. Mitchell,[1] G. J. Jenkins[1]

A comparison of observations with simulations of a coupled ocean-atmosphere general circulation model shows that both natural and anthropogenic factors have contributed significantly to 20th century temperature changes. The model successfully simulates global mean and large-scale land temperature variations, indicating that the climate response on these scales is strongly influenced by external factors. More than 80% of observed multidecadal-scale global mean temperature variations and more than 60% of 10- to 50-year land temperature variations are due to changes in external forcings. Anthropogenic global warming under a standard emissions scenario is predicted to continue at a rate similar to that observed in recent decades.

Over the last three decades, global mean temperature near Earth's surface has been increasing at a rate of 0.2 K/decade. This rise is unusually rapid compared to model estimates of natural internal variability (*1–3*). It is also unusual in the context of reconstructions of the past 1000 years from paleodata (*4, 5*). Simplified energy balance models of the climate system have been used to simulate global mean climate (*6, 7*), but they are not able to represent spatial patterns of temperature change, and their sensitivity must be tuned to fit the observations. Three-dimensional climate models are capable of producing good agreement with the observed warming of the last three decades if they include both greenhouse gases and the cooling effects of sulfate aerosols (*1, 8–10*).

A rise in near-surface temperatures as rapid as that during the last 30 years occurred over several decades during the first half of the 20th century, followed by a period of more than three decades when temperatures showed no long-term increase. The net radiative forcing of the atmosphere from the combined effects of greenhouse gases and sulfate aerosols is estimated to have increased more rapidly after 1960 than before (*8*). Consequently, climate models that include these two forcing factors alone have not generally been as successful at simulating climate change during the early part of the century. During this period, there were few explosive volcanic eruptions (*11*) and total solar irradiance was generally increasing from one solar cycle to the next (*12*), suggesting a possible natural origin of this warming trend. Various "detection and attribution" studies suggested that natural forcings may have contributed significantly to this early-century warming (*3, 9, 10, 13*), but the warming has also been attributed to an unusually large instance of internal variability (*2, 14*).

Here, we made an ensemble of simulations using a coupled ocean-atmosphere general circulation model that includes both the most important anthropogenic forcings and the most important natural forcings (*15*) during the 20th century. The model we use is HadCM3 (*16, 17*), a dynamical climate model which does not use flux adjustment (*18*). Our ensemble consists of four simulations that are identical except for their initial conditions. The initial conditions used were taken from states separated by 100 years in a 1300-year control run of HadCM3 in which external forcings have no year-to-year variations. The simulations in this ensemble incorporate changes in individual well-mixed greenhouse gases including carbon dioxide and methane (*19*), changes in tropospheric and stratospheric ozone, and changes in sulfur emissions. The direct effect of sulfate aerosols on planetary albedo is simulated using a fully interactive sulfur cycle scheme that models the emission, transport, oxidation, and removal of sulfur species. The indirect effect of tropospheric aerosol on cloud reflectivity (*20*) is also represented in the model. The simulations include natural forcings due to changes in the amount of stratospheric aerosols following explosive volcanic eruptions (*21*), and spectrally-resolved changes in solar irradiance (*22*). This ensemble is compared with two others; one of four simulations including the same anthropogenic forcings only and another of four simulations including the same natural forcings only. The three ensembles are named ALL, ANTHRO, and NATURAL, respectively.

The ALL ensemble captures the main features of global mean temperature changes observed since 1860 (Fig. 1, bottom). The approximately 0.2 K/decade rate of warming that is observed over the last three decades is reproduced by the model, and simulations and observations both show a similar rate of warming between 1910 and 1939. None of the NATURAL simulations shows a general warming over the last 30 years (Fig. 1, top), a period containing three major volcanic eruptions: Agung in 1963, El Chichón in 1982, and Mt. Pinatubo in 1991. In contrast, all four members of ANTHRO show warm-

[1]Met Office, Hadley Centre for Climate Prediction and Research, Bracknell, Berkshire RG12 2SY, UK. [2]Space Science and Technology Department, Rutherford Appleton Laboratory, Didcot, Oxfordshire OX11 0QX, UK and Department of Physics, University of Oxford, Oxford OX1 3PU, UK.

*To whom correspondence should be addressed. E-mail: pastott@meto.gov.uk